

# Spin excitations of the Shastry-Sutherland model – altermagnetism and proximate deconfined quantum criticality

Hongyu Chen,<sup>1,\*</sup> Guijing Duan,<sup>1,\*</sup> Changle Liu,<sup>2</sup> Yi Cui,<sup>1,3</sup> Weiqiang Yu,<sup>1,3</sup> Z. Y. Xie,<sup>1,3,†</sup> and Rong Yu<sup>1,3,‡</sup>

<sup>1</sup>*School of Physics and Beijing Key Laboratory of Opto-electronic Functional Materials and Micro-nano Devices, Renmin University of China, Beijing 100872, China*

<sup>2</sup>*School of Engineering, Dali University, Dali, Yunnan 671003, China*

<sup>3</sup>*Key Laboratory of Quantum State Construction and Manipulation (Ministry of Education), Renmin University of China, Beijing, 100872, China*

Symmetry plays a crucial role in condensed matter physics. In quantum magnetism, it dictates a number of exotic phenomena, including deconfined quantum criticality and altermagnetism. Here, by studying the spin excitations of the  $S = 1/2$  antiferromagnetic Shastry-Sutherland model, we show that the Néel antiferromagnetic state in this model is an altermagnet featuring a non-relativistic splitting between two chiral magnon bands. Moreover, we identify a Higgs mode in the longitudinal excitation channel, whose gap softens when approaching the antiferromagnetic to plaquette valence bond solid transition, implying the appearance of nearly deconfined excitations. However, the splitting between the two magnon bands (Goldstone modes) remains finite at the transition. These results indicate that the transition is weakly first-order and proximate to a putative deconfined quantum critical point. We find that the altermagnetism provides a sensitive means to probe the deconfined quantum criticality.

*Introduction.*—Symmetry is essential in physics. It provides an organizational principle to classify complex states of matter, and based on this, many exotic phenomena are understood [1–3]. One prominent example is the recently proposed altermagnet, a collinear antiferromagnetic (AFM) state in which the two sublattices with oppositely polarized spins are connected by the rotational symmetry instead of inversion or translation [4, 5]. The distinct symmetry, which is organized by the spin space group theory [6], causes a non-relativistic spin-dependent splitting of energy bands and may give rise to some exotic effects, such as anomalous Hall effect [4, 7]. Up to now, most studies focus on itinerant systems [8–10]. For insulating altermagnets, though a symmetry dictated splitting in magnon bands has been predicted [11], existing studies are mostly limited to several model systems [12–15].

Symmetry can also dictate phase transitions. In the Landau-Ginzburg-Wilson paradigm, a system transitions from a disordered state to an ordered one by spontaneously breaking a symmetry. With quantum fluctuations the transition can be continuous and occur at zero temperature, giving rise to intriguing quantum critical phenomena [16–26]. For a transition between two ordered phases, the Landau paradigm predicts a first-order transition. However, this scenario has recently been challenged. It was proposed that the transition between a valence bond solid (VBS) and an antiferromagnetic (AFM) phase can be continuous, *e.g.*, via a deconfined quantum critical point (DQCP) [18]. At the DQCP, the establishment of one order is accompanied by the destruction of the other order via proliferation of topological excitations, giving rise to emergent deconfined fractionalized excitations as well as enhanced continuous symmetry among the seemingly unrelated two types of order

parameters. This scenario has motivated extensive studies on DQCP [27–32]. However, whether a DQCP can be realized in quantum spin models is still an open question.

Tuning the frustration is a promising way to induce a VBS-to-AFM transition, and a prominent example is given by the Shastry-Sutherland (SS) model [33]. The model is defined on the SS lattice as illustrated in Fig. 1(a). It contains orthogonal spin dimers (with coupling  $J'$ ) connected by frustrated nearest neighbor (n.n.) bonds (with coupling  $J$ ). With increasing  $J/J'$ , the ground state experiences a series of quantum phase transitions from a dimer singlet phase to a plaquette VBS at  $J/J' \approx 0.68$ , then to a Néel AFM state for  $J/J' \sim 0.8$  (see Fig. 1(b)).[21, 34–41]. Although the dimer-to-plaquette transition is clearly strongly first-order, the nature of the plaquette-to-AFM transition remains elusive: Several tensor network calculations [37, 42] showed it to be weakly first-order, while some other study [39] found an intervening gapless quantum spin liquid in between the plaquette and AFM phases. Interestingly, one DMRG work [21] suggested the transition is via a DQCP with an emergent  $O(4)$  symmetry, and quantum scaling behavior near this point has been revealed by a finite-size tensor network analysis [43]. One prominent signature of a DQCP is the emergence of deconfined fractionalized spin excitations. Although spin excitations in both plaquette and AFM states have been extensively studied [44–47], whether deconfined excitations emerge at the transition is still unclear.

The phase diagram of the SS model well describes the evolution of low-temperature phases of the quasi-2D antiferromagnet  $\text{SrCu}_2(\text{BO}_3)_2$  under pressure tuning [34, 48–55], giving the hope to realize a DQCP in this material. Remarkably, a recent NMR study in this compound [19] reported an unusually large anomalous dimension  $\eta$  at

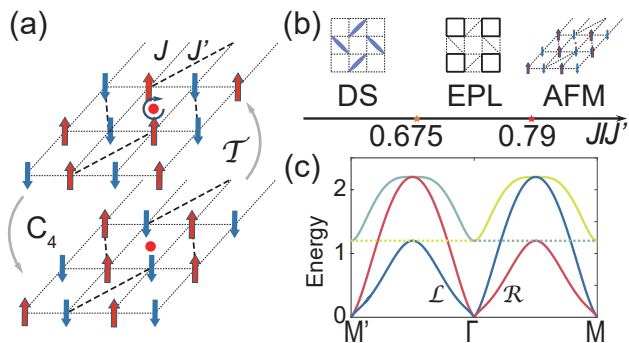


FIG. 1. (a): Sketch of the SS lattice and the corresponding altermagnetism. The two sublattices of the Néel state are connected by a  $C_4$  rotation of the lattice about the center of the empty plaquette (without the dimer bond). A time-reversal symmetry then recovers the Néel order. (b): Sketched phase diagram of the SS model with  $J/J'$ . The  $J/J'$  values at the two transitions are taken from Ref. [42]. (c): LSW dispersion in the AFM state of the SS model showing the chiral magnon bands with a non-zero splitting along the  $M'$ - $\Gamma$ - $M$  direction of the Brillouin zone.  $\mathcal{L}$ ( $\mathcal{R}$ ) refers to the left(right)-handed chiral magnon bands.

a field-induced plaquette-to-AFM transition under pressure, implying behavior in proximity to a DQCP. However, direct spectral evidence on the deconfined excitations at zero field is absent.

In this Letter, we study spin excitations of the SS model by using the state-of-the-art tensor network method for infinite lattice systems. This prevents from the severe finite-size effect in usual numerical calculations and offers a new perspective on the nature of emergent DQCP phenomena. We show that the altermagnetic nature of the AFM state causes a finite splitting with opposite chirality in the magnon bands along the  $\Gamma$  to  $M$  direction of the Brillouin zone. Besides the transverse excitations, we also identify a Higgs mode in the longitudinal excitation channel, whose energy decreases with reducing  $J/J'$  ratio. Approaching the plaquette-to-AFM transition, the gaps of the Higgs mode and the triplet excitations in the plaquette phase both rapidly drop close to zero, implying the emergence of nearly deconfined excitations. However, the splitting of the magnon bands remains finite at the transition. These results suggest the transition is weakly first-order, in proximity to a DQCP with an emergent  $O(4)$  symmetry. In general, we show that the split magnon bands caused by the altermagnetism serve as a sensitive probe for a deconfined quantum phase transition.

*Model and method.*—The Hamiltonian of the SS model reads as

$$\mathcal{H} = J \sum_{\langle i,j \rangle} \mathbf{S}_i \cdot \mathbf{S}_j + J' \sum_{\langle\langle i,j \rangle\rangle} \mathbf{S}_i \cdot \mathbf{S}_j, \quad (1)$$

where  $\mathbf{S}_i$  is an  $S = 1/2$  spin operator defined on site  $i$ ,  $J$  and  $J'$  are AFM inter- and intra-dimer cou-

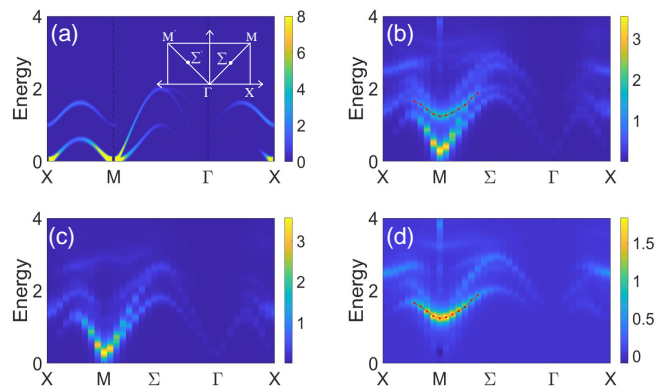


FIG. 2. (a): Spin DSF in the AFM phase of the SS model calculated by the LSW theory. The inset shows high symmetric directions of the Brillouin zone. (b): Total spin DSF ( $\mathcal{S}^{xx+yy+zz}$ ) in the AFM phase calculated by the iPEPS method with  $D = 3$  at  $J/J' = 1.1$ . (c): The transverse component ( $\mathcal{S}^{xx+yy}$ ) of the results in (b). (d): The longitudinal component ( $\mathcal{S}^{zz}$ ) of the results in (b). The dashed lines in (b) and (d) label the Higgs mode.

plings on the SS lattice, and we set  $J' = 1$  in this work. We apply the infinite projected entangled pair state (iPEPS) method [56–60] to calculate the ground states of the model. The iPEPS wavefunction is obtained by variationally minimizing the ground state energy using gradient-based optimization, where the gradients are calculated through the automatic differentiation technique [61, 62]. Then we construct the iPEPS ansatz for excited states through the single-mode approximation, and solve the generalized eigenvalue problem for the Hamiltonian in the tangent space spanned by these excited states [63–65]. Details of the methods are explained in the Supplemental Material (SM) [66]. With the information of the excited states, we calculate the spin dynamical structure factor (DSF)  $\mathcal{S}^{\alpha\beta}(\mathbf{q}, \omega) = \frac{1}{N} \sum_{i,j} \int dt e^{i\mathbf{q} \cdot (\mathbf{r}_i - \mathbf{r}_j)} e^{i\omega t} \langle S_i^\alpha(t) S_j^\beta(0) \rangle$ , where  $\alpha, \beta$  refer to the spin components. The excitation spectra are calculated within the tensor network states up to bond dimension  $D = 5$ . We also compare the results with linear spin wave (LSW) and bond-operator theories, which are introduced in detail in SM [66].

*Altermagnetism and chiral magnons in the SS model.*—The space group of the SS lattice is non-symmorphic and the two sublattices of the Néel AFM state are connected by neither translational nor inversion, but a  $C_4$  rotation about the center of the empty plaquette. The AFM order then recovers by further applying a time-reversal  $\mathcal{T}$  symmetry to the spins (see Fig. 1(a)). This indicates that the Néel AFM state on the SS lattice is an altermagnet with a  $d$ -wave symmetry. The spin space group symmetry dictates a non-zero splitting with opposite chirality of the magnon bands along the diagonal directions of the Brillouin zone. This is confirmed by the LSW calcula-

tion shown in Fig. 1(c). Along the  $M'-\Gamma-M$  direction, the acoustic (Goldstone) modes split into two branches with left- and right-handed chiralities, respectively. The splitting between the two chiral modes along  $\Gamma-M$  and  $\Gamma-M'$  directions has opposite sign, and its magnitude reaches a maximum at the mid-point  $\Sigma$  (and  $\Sigma'$ ). On the other hand, the two modes are degenerate along the  $\Gamma-X$  (and  $X-M$ ) directions (Fig. 2(a)). These properties verify that the altermagnet has a  $d$ -wave nature. Note that the optical modes also split, but one band is completely flat along the  $M'-\Gamma-M$  due to frustration and has zero spectral weight.

*Spin excitation spectra.*—We implement tensor network calculation to go beyond the LSW results on the spin excitation spectra. The calculated spectrum at  $J/J' = 1.1$  is shown in Fig. 2(b). It exhibits richer structures than the LSW results in Fig. 2(a). To understand these structures, we calculate the transverse and longitudinal components of the DSF,  $\mathcal{S}^{xx+yy}(\mathbf{q}, \omega)$  and  $\mathcal{S}^{zz}(\mathbf{q}, \omega)$ , and show them in Fig. 2(c) and (d), respectively. The transverse DSF resembles the LSW spectrum with three dispersive magnon bands. The finite gap at  $M$  (and  $\Gamma$ ) of the Goldstone modes is an effect of finite bond dimension  $D$  of the iPEPS ansatz, and vanishes in the large- $D$  limit (Fig.S3 of SM [66]). One prominent feature is the splitting of Goldstone modes along the  $\Gamma-M$  direction. The opposite sign of  $\Delta\mathcal{S} = \mathcal{S}^{+-}(\mathbf{q}, \omega) - \mathcal{S}^{-+}(\mathbf{q}, \omega)$  for the two modes shown in Fig.S4 justifies their opposite chirality, as expected for an altermagnet.

The spectrum of longitudinal modes, shown in Fig. 2(d), also consist of multiple bands, owing to the complex SS lattice structure (see discussion below). We can identify a mode (labeled by the dashed line) that develops a strong resonance at the  $M$  point. The energy of this mode decreases with reducing  $J/J'$  (see Fig.S2 of SM [66]). We then attribute it to the Higgs mode which reflects the amplitude fluctuations of the AFM order parameter. In a two-dimensional AFM state, the Higgs mode is usually hardly visible because the gapless Goldstone modes give rise to a divergent longitudinal susceptibility and the Higgs mode can decay into a pair of Goldstone modes [67]. Here it shows up in the tensor network calculation for the following reasons: The gapped Goldstone modes at finite  $D$  remove the divergence, and the single-mode approximation adopted suppresses the two-magnon continuum but preserves the two-magnon bound state, which is just the Higgs mode. Just above the Higgs mode, we find another longitudinal mode that is quasi-degenerate to the Higgs one at  $M$  point but develops a sizable separation at  $\Sigma$  point. Similar behavior was reported in a related model [15], and its origin needs further study. Besides the collective excitation modes discussed above, the spectrum also contains a continuum, as shown in the broad peak above about  $2J'$  in the density of states in Fig. S5 of SM [66]. Interestingly, the peak moves to lower energy when reducing  $J/J'$  toward the plaquette-

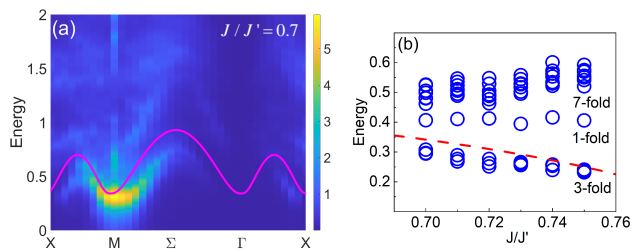


FIG. 3. (a): Spin DSF in the plaquette phase calculated by the iPEPS method with  $D = 3$  at  $J/J' = 0.7$ . The red dashed line labels the dispersion of the triplet excitations in the bond-operator theory. (b):  $J/J'$  dependence of extracted gaps at the  $M$  point of the Brillouin zone for several low-energy excitation modes in the plaquette phase, including, from bottom to top, a triplet, a singlet, and a 7-fold multiplet. The results are obtained by the iPEPS method with  $D = 4$ . The dashed line shows the gap of the triplet excitations in the bond-operator theory.

to-AFM transition, in a way similar to the behavior of the Higgs mode.

For a comprehensive understanding, we also study the excitations in the plaquette phase, and a typical spectrum at  $J/J' = 0.7$  is shown in Fig. 3(a). The lowest-energy excitations are found to be a triplet mode, whose dispersion can be described by the bond-operator theory [44, 66]. Fig. 3(b) illustrates excitation gaps at the  $M$  point of all identified low-energy modes, which, from bottom to top, include the triplet mode, one singlet mode, and a 7-fold multiplet. Note that the minor splitting probably comes from numerical accuracy and can be eliminated by enforcing the spin  $SU(2)$  symmetry in the calculation. The gap of the triplet mode decreases with increasing  $J/J'$  toward the plaquette-to-AFM transition and the gap size is comparable with that from the bond-operator theory. The energy of the singlet mode is almost independent of  $J/J'$ , and that of the 7-fold multiplet slightly increases with  $J/J'$ . We calculate the quantum numbers of the 7-fold multiplet and find that this multiplet consists of two triplets and one singlet, which are the eigenstates of a single plaquette (see Fig. S6 of SM [66]). The inter-plaquette interaction then couples multiplets in each plaquette into bands that can be understood by a generalized bond-operator theory [45]. Note that each triplet excitation will further split to transverse and longitudinal modes once the magnetic order breaks the spin  $SU(2)$  symmetry, accounting for the complex multiband structure shown in Fig. 2 in the AFM phase. The singlet excitation cannot be described within a single plaquette picture and is interpreted as an inter-plaquette bound state. Above these low-energy excitations, the spectrum becomes continuous above about  $J'$  (Fig. S5 of SM [66]), similar to the case of the AFM phase.

*Probing the DQCP.*—With excitations studied in both plaquette and AFM phases, we now understand the na-

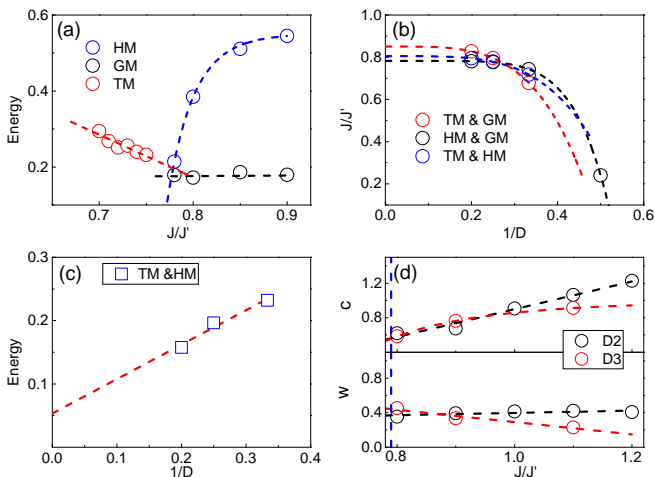


FIG. 4. (a): Gaps at the M point of the triplet mode (TM), Higgs mode (HM), and Goldstone modes (GM) with  $J/J'$  near the plaquette-to-AFM transition, obtained in the iPEPS calculation with  $D = 4$ . (b): Finite- $D$  analysis on the crossing points of the three types of excitation modes in (a). In the large- $D$  limit, all crossing points are close to the plaquette-to-AFM transition at  $(J/J')_c \approx 0.79$ , suggesting the transition is proximate to a (putative) DQCP. (c): Extrapolation of the energy of the crossing point between the Higgs mode and the triplet mode with  $1/D$ . The small energy in the large- $D$  limit indicates existence of nearly deconfined excitations. (d): Evolution of spin-wave velocities  $c$  and the anisotropic parameter  $w$  of the two Goldstone modes with  $J/J'$  in the AFM phase from the iPEPS calculation. Approaching the plaquette-to-AFM transition (indicated by the vertical dashed line),  $w$  remains to be finite, indicating non-degenerate Goldstone modes at the transition point.

ture of the plaquette-to-AFM transition. One signature of DQCP is that at the transition, the triplet mode and Higgs mode should both become gapless and degenerate to the Goldstone modes. In Fig. 4(a) we plot the extracted gaps of the triplet mode, Higgs mode, and Goldstone modes at the M point with bond dimension  $D = 4$ . The gaps for other  $D$  values are presented in Fig. S7 of the SM [66]. The gap of the Goldstone modes is almost independent of  $J/J'$ , indicating that the gap is caused by finite  $D$ . On the other hand, gaps of both triplet mode and Higgs mode drop rapidly and are close to the gap of the Goldstone modes when approaching the transition point  $(J/J')_c \approx 0.79$ . [42] The crossing points of these modes are all close to  $(J/J')_c$  when extrapolating to the large- $D$  limit, as shown in Fig. 4(b). These behaviors imply proximity to a continuous quantum phase transition with nearly deconfined excitations. However, detailed analysis shows the crossing point of Higgs mode and Goldstone modes is at  $J/J' < (J/J')_c$  at  $D \rightarrow \infty$ , while the one of triplet mode and Goldstone modes is at  $J/J' > (J/J')_c$ . This suggests that both Higgs mode and triplet mode are still gapped when extrapolating to the transition point. Indeed, as shown in Fig. 4(c), the en-

ergy of the crossing point between Higgs mode and triplet mode is about  $0.05J'$ , a small gap close to zero.

Interestingly, we find the nature of the plaquette-to-AFM transition can be detected by the splitting of the two Goldstone modes. The DQCP theory for the SS model proposed the emergence of an  $O(4)$  symmetry between the AFM and plaquette order parameters [21]. According to this theory, the Higgs mode and the two Goldstone modes would be degenerate and become the lower edge of the deconfined spinon continuum  $\omega_{\min}(\mathbf{q}) \sim J|\mathbf{q}|$  at the DQCP. However, because the Néel AFM state of the SS model is an altermagnet, splitting between the two chiral Goldstone modes should be present when the AFM order parameter is finite. The splitting at the transition point vanishes only if the transition is continuous, via a DQCP. We fit the dispersions of the two Goldstone modes along the  $\Gamma$ -M direction by  $\omega_{\pm}(\mathbf{q}) = \sqrt{\Delta^2 + c^2 q^2} \pm w q_x q_y$ , where  $c$  refers to the spin-wave velocity in the gapless ( $\Delta \rightarrow 0$ ) limit. The  $w$  term accounts for the split Goldstone modes in the altermagnet with a  $d$ -wave symmetry where  $w$  is an anisotropic parameter. The fitted  $c$  and  $w$  parameters are shown in Fig. 4(d). Approaching the transition, both of them are finite. This indicates that well-defined Goldstone modes with a non-zero splitting persist at the transition point. Together with the small gap of Higgs mode approaching the transition, the numerical results suggest the plaquette-to-AFM transition is weakly first-order and proximate to a DQCP.

*Discussions and conclusions.*—To understand the numerical results, note that the splitting of the Goldstone modes is caused by the  $d$ -wave anisotropic  $w$  term in the  $q^2$  order of the magnon dispersions. The Goldstone modes are still degenerate up to the linear-in- $q$  term. Therefore, one argues that the  $w$  term, though a symmetry-breaking perturbation, is irrelevant in the low-energy effective theory, which predicts a DQCP with an emergent  $O(4)$  symmetry. However, given that the  $O(4)$  DQCP is obtained by deforming an  $SO(5)$  conformal field theory (CFT) along a particular direction [21] and the  $SO(5)$  CFT could be non-unitary [68–70], realization of an  $O(4)$  DQCP on a lattice model would be delicate. Most likely, perturbations reflecting the exact lattice symmetry would eventually make the DQCP proximate.

This proximate DQCP scenario is supported by the appearance of rich low-lying modes on both sides when approaching the transition. These include the softening of the triplet mode in the plaquette phase and the Higgs mode in the AFM phase. In addition, we also observe a singlet excitation in the plaquette phase and quasi-degenerate longitudinal modes in the AFM phase. The appearance of more than three low-energy excitations on either side of the transition suggests that it goes beyond the conventional  $O(3)$  Wilson-Fisher universality or an  $O(4)$  symmetry-enhanced first-order transition, but is instead proximate to a putative  $O(4)$  DQCP, which

supports both soft  $S = 1$  and  $S = 0$  modes. Moreover, our scenario naturally applies to a large class of models including the SS model, the Heisenberg model on the checkerboard lattice, the checkerboard  $J$ - $Q$  model, and their variants, all of which hold a  $d$ -wave altermagnetic phase dictated by the  $C_4\mathcal{T}$  symmetry. The proximity to a putative DQCP provides a unified explanation for the observed quantum scaling behaviors at the plaquette-to-AFM transition in both the SS model [43] and the checkerboard  $J$ - $Q$  model [71, 72]. It would be interesting to understand how the spin frustration influences the transition by systematically studying the excitation spectra of these models.

We have examined the lattice structure of the SS model material  $\text{SrCu}_2(\text{BO}_3)_2$ , and find that the structure indeed supports an altermagnet even when the non-magnetic ions are included. Our proximate DQCP scenario then applies: The transition is weakly first-order and proximate to a putative DQCP. Indeed this has been observed in a recent NMR experiment under finite magnetic field [19] and a study on the specific heat at zero field [73].

Besides the DQCP, another unsettled issue is the nature of the plaquette state. Recent inelastic neutron scattering (INS) [52] and NMR [19] measurements suggest a full plaquette phase where the singlet is located on the plaquette with a  $J'$  dimer. But most numerical results (including ours) on the SS model found the ground state is an empty plaquette (without the  $J'$  dimer). Interestingly, for the plaquette state at  $J/J' = 0.7$ , if taking  $J' \sim 4$  meV estimated from the experiment, the calculated spin gaps of the lowest triplet mode and the 7-fold degenerate mode (including two degenerate triplets) are about 1 meV and 2 meV, which are consistent with the gap values of the lowest two excitations observed in the INS experiment [52]. It would be important to further compare the theoretical and experimental results on the dispersions and evolution of the spin gaps with pressure.

To experimentally probe the altermagnetism, one may look for the splitting of the two magnon bands (at the order of  $J'$  near the  $\Sigma$  point) in the spectrum of INS. The chiral magnons can be detected by resonant inelastic X-ray scattering (RIXS). Moreover, the transverse spin current induced by the chiral magnons will cause sizable spin Nernst effect in the AFM state [5, 74] when applying a temperature gradient along the non-splitting direction. Given that the Dzyaloshinsky-Moriya interaction is much smaller than  $J$  and  $J'$  in  $\text{SrCu}_2(\text{BO}_3)_2$ , the leading contribution should be attributed to the altermagnetism. Given that the splitting of the magnon bands in the altermagnetic phase is directly related to the  $O(4)$  symmetry breaking in the magnetic sector, the proposed experiments above, provide viable ways to detect the proximate deconfined quantum criticality.

In conclusion, we study the spin excitations of the SS model by using advanced tensor network method. We

show that the antiferromagnetic state of the model is an altermagnet supporting two split magnons (Goldstone modes) with opposite chirality. Besides the Goldstone modes, we also identify a Higgs mode in the longitudinal channel. The spin excitations in the plaquette singlet phase contain several triplet modes. The dispersion of the lowest-energy triplet mode can be described by the bond-operator theory. When the system approaches the transition, rich excitations appear in low energies, and the gaps of both the Higgs and the triplet excitations reduce rapidly close to zero. These suggest emergence of nearly deconfined excitations. However, the splitting between the two Goldstone modes, caused by the altermagnetism, remains at the transition point, indicating that the transition is weakly first-order and proximate to a putative deconfined quantum critical point. Our results indicate that the altermagnetism of the system has an interesting interplay with the deconfined quantum criticality and provides viable means of detecting this exotic phase transition.

*Acknowledgments.*— We thank Runze Chi, Wenan Guo, Bruce Normand, Wei Li, Zhengxin Liu, Anders W. Sandvik, Yiming Wang, Jize Zhao for helpful discussions. This work is supported by the National Key R&D Program of China (Grant No. 2023YFA1406500), the National Natural Science Foundation of China (Grant Nos. 12334008, 12274458, 12174441).

---

\* These authors contributed equally to the work.

† qingtaoxie@ruc.edu.cn

‡ rong.yu@ruc.edu.cn

- [1] M Zahid Hasan and Charles L Kane. Colloquium: topological insulators. *Reviews of modern physics*, 82(4):3045–3067, 2010.
- [2] Todadri Senthil. Symmetry-protected topological phases of quantum matter. *Annu. Rev. Condens. Matter Phys.*, 6(1):299–324, 2015.
- [3] Edward Witten. Symmetry and emergence. *Nature Physics*, 14(2):116–119, 2018.
- [4] Libor Šmejkal, Jairo Sinova, and Tomas Jungwirth. Emerging research landscape of altermagnetism. *Physical Review X*, 12(4):040501, 2022.
- [5] Libor Šmejkal, Jairo Sinova, and Tomas Jungwirth. Beyond conventional ferromagnetism and antiferromagnetism: A phase with nonrelativistic spin and crystal rotation symmetry. *Physical Review X*, 12(3):031042, 2022.
- [6] Jian Yang, Zheng-Xin Liu, and Chen Fang. Symmetry invariants and classes of quasi-particles in magnetically ordered systems having weak spin-orbit coupling. *arXiv preprint arXiv:2105.12738*, 2021.
- [7] Libor Šmejkal, Allan H MacDonald, Jairo Sinova, Satoru Nakatsuji, and Tomas Jungwirth. Anomalous hall antiferromagnets. *Nature Reviews Materials*, 7(6):482–496, 2022.
- [8] RD Gonzalez Betancourt, Jan Zubáč, R Gonzalez-Hernandez, Kevin Geishendorf, Zbynek Šobáň, Gunther Springholz, Kamil Olejník, Libor Šmejkal, Jairo Sinova,



- Tomas Jungwirth, et al. Spontaneous anomalous hall effect arising from an unconventional compensated magnetic phase in a semiconductor. *Physical Review Letters*, 130(3):036702, 2023.
- [9] A Hariki, A Dal Din, OJ Amin, T Yamaguchi, A Badura, D Kriegner, KW Edmonds, RP Champion, P Wadley, D Backes, et al. X-ray magnetic circular dichroism in altermagnetic  $\alpha$ -mnte. *Physical Review Letters*, 132(17):176701, 2024.
- [10] Francesco Ferrari and Roser Valenti. Altermagnetism on the shastry-sutherland lattice. *arXiv preprint arXiv:2408.00841*, 2024.
- [11] Libor Šmejkal, Alberto Marmodoro, Kyo-Hoon Ahn, Rafael González-Hernández, Ilja Turek, Sergiy Mankovsky, Hubert Ebert, Sunil W D'Souza, Ondřej Šipr, Jairo Sinova, et al. Chiral magnons in altermagnetic ruo 2. *Physical Review Letters*, 131(25):256703, 2023.
- [12] Hai-Yang Ma and Jin-Feng Jia. Altermagnetic topological insulator and the selection rules. *Physical Review B*, 110(6):064426, 2024.
- [13] Markus Weißenhofer and Alberto Marmodoro. Atomistic spin dynamics simulations of magnonic spin seebeck and spin nernst effects in altermagnets. *Physical Review B*, 110(9):094427, 2024.
- [14] Meng-Han Zhang, Lu Xiao, and Dao-Xin Yao. Topological magnons in a collinear altermagnet. *arXiv preprint arXiv:2407.18379*, 2024.
- [15] Yang Liu, Shiqi Shao, Saisai He, Z. Y. Xie, Jia-Wei Mei, Hong-Gang Luo, and Jize Zhao. Quantum dynamics in a spin-1/2 square lattice  $j_1$ - $j_2$ - $\delta$  altermagnet. *arXiv preprint arXiv:2410.06955*, 2024.
- [16] Subir Sachdev and Bernhard Keimer. Quantum criticality. *Physics Today*, 64(2):29–35, 2011.
- [17] Radu Coldea, DA Tennant, EM Wheeler, E Wawrzynska, D Prabhakaran, M Telling, K Habicht, P Smeibidl, and K Kiefer. Quantum criticality in an ising chain: experimental evidence for emergent e8 symmetry. *Science*, 327(5962):177–180, 2010.
- [18] T. Senthil, Ashvin Vishwanath, Leon Balents, Subir Sachdev, and Matthew P. A. Fisher. Deconfined quantum critical points. *Science*, 303(5663):1490–1494, 2004.
- [19] Yi Cui, Lu Liu, Huihang Lin, Kai-Hsin Wu, Wenshan Hong, Xuefei Liu, Cong Li, Ze Hu, Ning Xi, Shiliang Li, et al. Proximate deconfined quantum critical point in srCu<sub>2</sub>(bo<sub>3</sub>)<sub>2</sub>. *Science*, 380(6650):1179–1184, 2023.
- [20] Y Cui, H Zou, N Xi, Zhangzhen He, YX Yang, L Shu, GH Zhang, Z Hu, T Chen, Rong Yu, et al. Quantum criticality of the ising-like screw chain antiferromagnet srCo<sub>2</sub>v<sub>2</sub>o<sub>8</sub> in a transverse magnetic field. *Physical Review Letters*, 123(6):067203, 2019.
- [21] Jong Yeon Lee, Yi Zhuang You, Subir Sachdev, and Ashvin Vishwanath. Signatures of a Deconfined Phase Transition on the Shastry-Sutherland Lattice: Applications to Quantum Critical SrCu<sub>2</sub>(BO<sub>3</sub>)<sub>2</sub>. *Physical Review X*, 9, 11 2019.
- [22] Haiyuan Zou, Yi Cui, Xiao Wang, Z Zhang, J Yang, Guangyong Xu, A Okutani, M Hagiwara, M Matsuda, G Wang, et al. E 8 spectra of quasi-one-dimensional antiferromagnet baco 2 v 2 o 8 under transverse field. *Physical review letters*, 127(7):077201, 2021.
- [23] Y Xu, LS Wang, YY Huang, JM Ni, CC Zhao, YF Dai, BY Pan, XC Hong, P Chauhan, SM Koohpayeh, et al. Quantum critical magnetic excitations in spin-1/2 and spin-1 chain systems. *Physical Review X*, 12(2):021020, 2022.
- [24] Utkarsh Agrawal, Sarang Gopalakrishnan, and Romain Vasseur. Quantum criticality in the 2d quasiperiodic potts model. *Physical review letters*, 125(26):265702, 2020.
- [25] Sebastian Fey, Sebastian C Kapfer, and Kai Phillip Schmidt. Quantum criticality of two-dimensional quantum magnets with long-range interactions. *Physical review letters*, 122(1):017203, 2019.
- [26] Xibo Zhang, Chen-Lung Hung, Shih-Kuang Tung, Nathan Gemelke, and Cheng Chin. Exploring quantum criticality based on ultracold atoms in optical lattices. *New Journal of Physics*, 13(4):045011, 2011.
- [27] Anders W. Sandvik. Evidence for deconfined quantum criticality in a two-dimensional heisenberg model with four-spin interactions. *Phys. Rev. Lett.*, 98:227202, Jun 2007.
- [28] Nvsen Ma, Guang-Yu Sun, Yi-Zhuang You, Cenke Xu, Ashvin Vishwanath, Anders W Sandvik, and Zi Yang Meng. Dynamical signature of fractionalization at a deconfined quantum critical point. *Physical Review B*, 98(17):174421, 2018.
- [29] Hui Shao, Wenan Guo, and Anders W Sandvik. Quantum criticality with two length scales. *Science*, 352(6282):213–216, 2016.
- [30] T Senthil, Matthias Vojta, and Subir Sachdev. Weak magnetism and non-fermi liquids near heavy-fermion critical points. *Physical Review B*, 69(3):035111, 2004.
- [31] Zi Hong Liu, Matthias Vojta, Fakher F Assaad, and Lukas Janssen. Metallic and deconfined quantum criticality in dirac systems. *Physical Review Letters*, 128(8):087201, 2022.
- [32] Zehui Deng, Lu Liu, Wenan Guo, and Hai-Qing Lin. Diagnosing quantum phase transition order and deconfined criticality via entanglement entropy. *Physical Review Letters*, 133(10):100402, 2024.
- [33] B. Sriram Shastry and Bill Sutherland. Exact ground state of a quantum mechanical antiferromagnet. *Physica B+C*, 108(1):1069–1070, 1981.
- [34] Akihisa Koga and Norio Kawakami. Quantum Phase Transitions in the Shastry-Sutherland Model for SrCu<sub>2</sub>(BO<sub>3</sub>)<sub>2</sub>. *Phys. Rev. Lett.*, 84:4461–4464, May 2000.
- [35] C. H. Chung, J. B. Marston, and Subir Sachdev. Quantum phases of the shastry-sutherland antiferromagnet: Application to (formula presented). *Physical Review B - Condensed Matter and Materials Physics*, 64, 2001.
- [36] J. H. Pixley, Rong Yu, and Qimiao Si. Quantum phases of the shastry-sutherland kondo lattice: Implications for the global phase diagram of heavy-fermion metals. *Phys. Rev. Lett.*, 113:176402, Oct 2014.
- [37] Philippe Corboz and Frédéric Mila. Tensor network study of the shastry-sutherland model in zero magnetic field. *Phys. Rev. B*, 87:115144, Mar 2013.
- [38] C. Boos, S. P.G. Crone, I. A. Niesen, P. Corboz, K. P. Schmidt, and F. Mila. Competition between intermediate plaquette phases in SrCu<sub>2</sub>(BO<sub>3</sub>)<sub>2</sub> under pressure. *Physical Review B*, 100, 10 2019.
- [39] Jianwei Yang, Anders W. Sandvik, and Ling Wang. Quantum criticality and spin liquid phase in the shastry-sutherland model, 2021.
- [40] Keola Wierschem and Pinaki Sengupta. Columnar antiferromagnetic order and spin supersolid phase on the extended shastry-sutherland lattice. *Physical review let-*

- ters, 110(20):207207, 2013.
- [41] Junsen Wang, Han Li, Ning Xi, Yuan Gao, Qing-Bo Yan, Wei Li, and Gang Su. Plaquette singlet transition, magnetic barocaloric effect, and spin supersolidity in the shastry-sutherland model. *Physical Review Letters*, 131(11):116702, 2023.
- [42] Ning Xi, Hongyu Chen, ZY Xie, and Rong Yu. Plaquette valence bond solid to antiferromagnet transition and deconfined quantum critical point of the shastry-sutherland model. *Physical Review B*, 107(22):L220408, 2023.
- [43] Wen-Yuan Liu, Xiao-Tian Zhang, Zhe Wang, Shou-Shu Gong, Wei-Qiang Chen, and Zheng-Cheng Gu. Quantum criticality with emergent symmetry in the extended shastry-sutherland model. *Physical Review Letters*, 133(2):026502, 2024.
- [44] M Moliner, Ioannis Rousochatzakis, and Frederic Mila. Emergence of one-dimensional physics from the distorted shastry-sutherland lattice. *Physical Review B—Condensed Matter and Materials Physics*, 83(14):140414, 2011.
- [45] Zhifeng Zhang and Pinaki Sengupta. Generalized plaquette state in the anisotropic shastry-sutherland model. *Physical Review B*, 92(9):094440, 2015.
- [46] Zhentao Wang and Cristian D Batista. Dynamics and instabilities of the shastry-sutherland model. *Physical Review Letters*, 120(24):247201, 2018.
- [47] Ke Liu and Fa Wang. Schwinger boson symmetric spin liquids of shastry-sutherland model. *Physical Review B*, 109(13):134409, 2024.
- [48] H. Kageyama, K. Yoshimura, R. Stern, N. V. Mushnikov, K. Onizuka, M. Kato, K. Kosuge, C. P. Slichter, T. Goto, and Y. Ueda. Exact Dimer Ground State and Quantized Magnetization Plateaus in the Two-Dimensional Spin System  $\text{SrCu}_2(\text{BO}_3)_2$ . *Phys. Rev. Lett.*, 82:3168–3171, Apr 1999.
- [49] Shin Miyahara and Kazuo Ueda. Exact Dimer Ground State of the Two Dimensional Heisenberg Spin System  $\text{SrCu}_2(\text{BO}_3)_2$ . *Phys. Rev. Lett.*, 82:3701–3704, May 1999.
- [50] Takeshi Waki, Koichi Arai, Masashi Takigawa, Yuta Saiga, Yoshiya Uwatoko, Hiroshi Kageyama, and Yutaka Ueda. A novel ordered phase in  $\text{SrCu}_2(\text{BO}_3)_2$  under high pressure. *Journal of the Physical Society of Japan*, 76, 7 2007.
- [51] S Haravifard, D Graf, AE Feiguin, CD Batista, JC Lang, DM Silevitch, G Srajer, BD Gaulin, HA Dabkowska, and TF Rosenbaum. Crystallization of spin superlattices with pressure and field in the layered magnet  $\text{SrCu}_2(\text{BO}_3)_2$ . *Nature communications*, 7(1):1–6, 2016.
- [52] M. E. Zayed, C. Rüegg, J. Larrea, A. M. Läuchli, C. Panagopoulos, S. S. Saxena, M. Ellerby, D. F. Mcmorrow, Th Strässle, S. Klotz, G. Hamel, R. A. Sadykov, V. Pomjakushin, M. Boehm, M. Jiménez-Ruiz, A. Schneidewind, E. Pomjakushina, M. Stingaciu, K. Conder, and H. M. Rønnow. 4-spin plaquette singlet state in the Shastry-Sutherland compound  $\text{SrCu}_2(\text{BO}_3)_2$ . *Nature Physics*, 13:962–966, 10 2017.
- [53] S. Bettler, L. Stoppel, Z. Yan, S. Gvasaliya, and A. Zheludev. Sign switching of dimer correlations in  $\text{SrCu}_2(\text{BO}_3)_2$  under hydrostatic pressure. *Phys. Rev. Research*, 2:012010, Jan 2020.
- [54] Jing Guo, Guangyu Sun, Bowen Zhao, Ling Wang, Wenshan Hong, Vladimir A. Sidorov, Nvsen Ma, Qi Wu, Shiliang Li, Zi Yang Meng, Anders W. Sandvik, and Lil-ing Sun. Quantum Phases of  $\text{SrCu}_2(\text{BO}_3)_2$  from High-Pressure Thermodynamics. *Phys. Rev. Lett.*, 124:206602, May 2020.
- [55] J. Larrea Jiménez, S. P. G. Crone, E. Fogh, M. E. Zayed, R. Lortz, E. Pomjakushina, K. Conder, A. M. Läuchli, L. Weber, S. Wessel, and et al. A quantum magnetic analogue to the critical point of water. *Nature*, 592(7854):370–375, Apr 2021.
- [56] Frank Verstraete and J Ignacio Cirac. Renormalization algorithms for quantum-many body systems in two and higher dimensions. *arXiv preprint cond-mat/0407066*, 2004.
- [57] Román Orús. A practical introduction to tensor networks: Matrix product states and projected entangled pair states. *Annals of physics*, 349:117–158, 2014.
- [58] Philippe Corboz, T Maurice Rice, and Matthias Troyer. Competing states in the t-j model: Uniform d-wave state versus stripe state. *Physical review letters*, 113(4):046402, 2014.
- [59] Román Orús and Guifré Vidal. Simulation of two-dimensional quantum systems on an infinite lattice revisited: Corner transfer matrix for tensor contraction. *Physical Review B*, 80(9):094403, 2009.
- [60] Philippe Corboz, Steven R. White, Guifré Vidal, and Matthias Troyer. Stripes in the two-dimensional t-j model with infinite projected entangled-pair states. *Physical Review B*, 84:041108, Jul 2011.
- [61] Bin-Bin Chen, Yuan Gao, Yi-Bin Guo, Yuzhi Liu, Hui-Hai Zhao, Hai-Jun Liao, Lei Wang, Tao Xiang, Wei Li, and Z. Y. Xie. Automatic differentiation for second renormalization of tensor networks. *Phys. Rev. B*, 101:220409, Jun 2020.
- [62] Hai-Jun Liao, Jin-Guo Liu, Lei Wang, and Tao Xiang. Differentiable programming tensor networks. *Physical Review X*, 9(3):031041, 2019.
- [63] Boris Ponsioen and Philippe Corboz. Excitations with projected entangled pair states using the corner transfer matrix method. *Physical Review B*, 101(19):195109, 2020.
- [64] Boris Ponsioen, Fakher F Assaad, and Philippe Corboz. Automatic differentiation applied to excitations with projected entangled pair states. *SciPost Physics*, 12(1):006, 2022.
- [65] Runze Chi, Yang Liu, Yuan Wan, Hai-Jun Liao, and T Xiang. Spin excitation spectra of anisotropic spin-1/2 triangular lattice heisenberg antiferromagnets. *Physical Review Letters*, 129(22):227201, 2022.
- [66] See supplemental material <http://link...> for details about the tensor network method, the linear spin wave theory, the bond-operator theory, and additional results on the spin excitation spectra, which also includes refs.[56–65, 75–78].
- [67] Daniel Podolsky, Assa Auerbach, and Daniel P Arovav. Visibility of the amplitude (higgs) mode in condensed matter. *Physical Review B—Condensed Matter and Materials Physics*, 84(17):174522, 2011.
- [68] Ruochen Ma and Chong Wang. Theory of deconfined pseudocriticality. *Physical Review B*, 102(2):020407, 2020.
- [69] Adam Nahum. Note on wess-zumino-witten models and quasiuniversality in 2+ 1 dimensions. *Physical Review B*, 102(20):201116, 2020.
- [70] Zheng Zhou, Liangdong Hu, W Zhu, and Yin-Chen He. So (5) deconfined phase transition under the fuzzy-sphere microscope: Approximate conformal symmetry, pseudo-

- criticality, and operator spectrum. *Physical Review X*, 14(2):021044, 2024.
- [71] Bowen Zhao, Phillip Weinberg, and Anders W Sandvik. Symmetry-enhanced discontinuous phase transition in a two-dimensional quantum magnet. *Nature Physics*, 15(7):678–682, 2019.
- [72] Chengchen Li, Huihang Lin, and Rong Yu. Quantum scaling of the spin lattice relaxation rate in the checkerboard j<sub>q</sub> model. *Journal of Physics: Condensed Matter*, 36(35):355805, 2024.
- [73] Jing Guo, Pengyu Wang, Cheng Huang, Bin-Bin Chen, Wenshan Hong, Shu Cai, Jinyu Zhao, Jinyu Han, Xintian Chen, Yazhou Zhou, et al. Deconfined quantum critical point lost in pressurized srCu<sub>2</sub>(bo<sub>3</sub>)<sub>2</sub>. *arXiv preprint arXiv:2310.20128*, 2023.
- [74] Qirui Cui, Bowen Zeng, Ping Cui, Tao Yu, and Hongxin Yang. Efficient spin seebeck and spin nernst effects of magnons in altermagnets. *Physical Review B*, 108(18):L180401, 2023.
- [75] X. F. Liu, Y. F. Fu, W. Q. Yu, J. F. Yu, and Z. Y. Xie. Variational corner transfer matrix renormalization group method for classical statistical models. *Chinese Physics Letters*, 39(6):067502, jun 2022.
- [76] J. Nocedal and S. J. Wright. *Numerical Optimization*. Springer New York, NY, 3 edition, 2006.
- [77] ME Zhitomirsky and Kazuo Ueda. Valence-bond crystal phase of a frustrated spin-1/2 square-lattice antiferromagnet. *Physical Review B*, 54(13):9007, 1996.
- [78] Subir Sachdev and RN Bhatt. Bond-operator representation of quantum spins: Mean-field theory of frustrated quantum heisenberg antiferromagnets. *Physical Review B*, 41(13):9323, 1990.



# SUPPLEMENTAL MATERIAL – Spin excitations of the Shastry-Sutherland model – altermagnetism and proximate deconfined quantum criticality

Hongyu Chen<sup>1</sup>, Guijing Duan<sup>1</sup>, Changle Liu<sup>2</sup>, Yi Cui<sup>1,3</sup>, Weiqiang Yu<sup>1,3</sup>, Z.Y.Xie<sup>1,3</sup>, Rong Yu<sup>1,3</sup>

<sup>1</sup>*School of Physics and Beijing Key Laboratory of Opto-electronic Functional Materials and Micro-nano Devices, Renmin University of China, Beijing 100872, China*

<sup>2</sup>*School of Engineering, Dali University, Dali, Yunnan 671003, China*

<sup>3</sup>*Key Laboratory of Quantum State Construction and Manipulation (Ministry of Education), Renmin University of China, Beijing, 100872, China*

## IPEPS METHOD FOR CALCULATING THE GROUND STATE AND EXCITED STATES

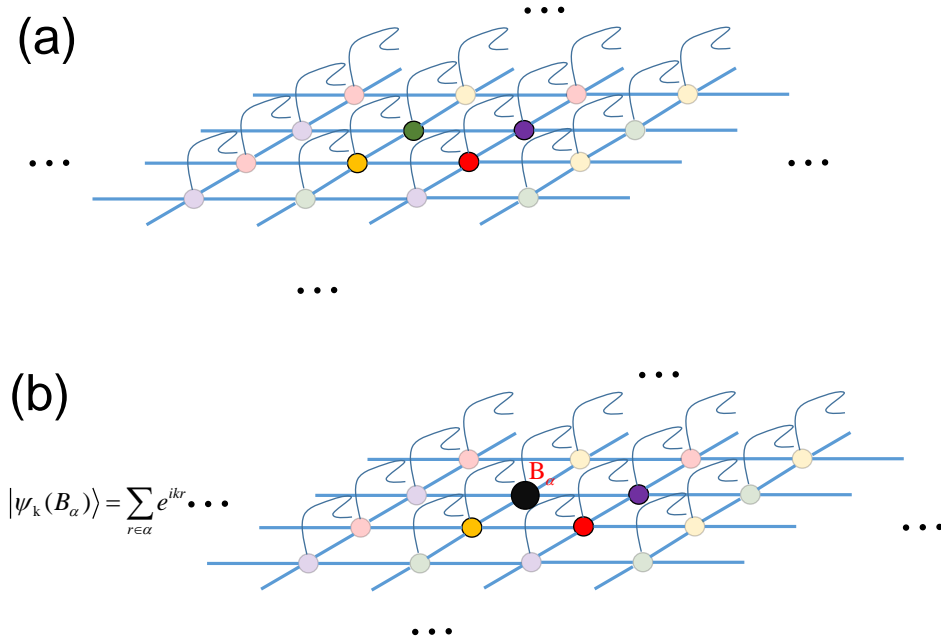


FIG. S-1. (a): The iPEPS setup in the calculation of the ground state of the SS model. The tensors are arranged at the sites of the SS lattice. The bright-colored sites indicate a  $2 \times 2$  unit cell used in the calculation. (b): Illustration of the single-mode iPEPS ansatz for the calculation of excited states. In each term of the summation, a single local tensor  $A_\alpha$  located at site  $r$  belonging to a specified sublattice is modified to a different tensor  $B_\alpha$ . Here  $\alpha = 1, 2, 3, 4$ , corresponding to a  $2 \times 2$  unit cell.

In this work, we apply the infinite projected entangled pair state (iPEPS) method [56, 57] to calculate the ground state of the Shastry-Sutherland (SS) model. A sketched iPEPS setup with a  $2 \times 2$  unit cell is shown in Fig. S-1(a). In the iPEPS setup, a local tensor is defined on each site of the SS lattice. As shown in Fig. S-1, each local tensor has a physical index corresponding to the spin degrees of freedom, with dimension 2 and denoted as curve, and four virtual indices corresponding to the four links of the site, with dimension  $D$  referred to as the iPEPS bond dimension and denoted as straight. In this work, as emphasized as bright color in Fig. S-1, the unit cell is chosen to be  $2 \times 2$ , and this is the minimal size compatible with the ground state of the SS model.

Given an iPEPS state  $|\Psi\rangle$ , the ground state energy can be evaluated according to the fundamental quantum mechanics

$$E = \frac{\sum_{\langle ij \rangle} \langle \Psi | \hat{H}_{ij}(J) | \Psi \rangle}{\langle \Psi | \Psi \rangle} + \frac{\sum_{\langle\langle ij \rangle\rangle} \langle \Psi | \hat{H}_{ij}(J') | \Psi \rangle}{\langle \Psi | \Psi \rangle} \quad (\text{S-1})$$

where  $\langle ij \rangle$  and  $\langle\langle ij \rangle\rangle$  denote nearest neighbors and second nearest neighbors, respectively. In this sense, the energy can be regarded as a complicated function of the local tensors, the variational parameters in the iPEPS ansatz.

The denominators and numerators in Eq. (S-1) can be effectively calculated by using the corner transfer matrix renormalization group method [58–60, 75]. Then, starting from an arbitrary state, the ground state is obtained by variationally minimizing the energy through gradient-based optimization, e.g., the L-BFGS optimization strategy [76]. In this work, the energy gradients concerning the local tensors are obtained effectively by the automatic differentiation techniques [61, 62].

Once the ground state  $|\Psi_0\rangle$  is obtained, we can construct the iPEPS ansatz for the excited state through the single-mode approximation [63–65]. More specifically, the excited ansatz with lattice momentum  $k$  reads as

$$|\Psi_k(B_\alpha)\rangle = \sum_{r \in \alpha} e^{ikr} |\Psi_r(B_\alpha)\rangle \quad (\text{S-2})$$

where  $\alpha$  denotes the four sublattices corresponding to the  $2 \times 2$  unit cell, and the summation is over all the sites belonging to the  $\alpha$ -th sublattice. Here  $|\Psi_r(B_\alpha)\rangle$  is the perturbed  $|\Psi_0\rangle$  state obtained by replacing the local tensor  $A_\alpha$  at  $r$  in  $|\Psi_0\rangle$  by a different tensor  $B_\alpha$ , which satisfies the orthogonal condition

$$\langle \Psi_r(B_\alpha) | \Psi_0 \rangle = 0. \quad (\text{S-3})$$

In practice,  $B_\alpha$  can be chosen to be a vector in the null space of  $E_\alpha$ , which is the effective environment of  $A_\alpha$  in  $\langle \Psi_0 | \Psi_0 \rangle$  and satisfies  $\langle \Psi_0 | \Psi_0 \rangle = \text{Tr} E_\alpha A_\alpha$ . For a given ground state with bond dimension  $D$ , we have  $2D^4 - 1$  choices of  $B_\alpha$  satisfying Eq.(S-3) for each  $\alpha$ , and thus  $8D^4 - 4$  basis vectors, denoted as  $|\Phi_i(k)\rangle$ , in total to span the tangent space of the ground state. Then, we can calculate the matrix representation of the Hamiltonian in this non-orthogonal basis, and solving the generalized eigenvalue equation

$$\langle \Psi_i(k) | \hat{H} | \Psi_j(k) \rangle = E(k) \langle \Psi_i(k) | \Psi_j(k) \rangle \quad (\text{S-4})$$

gives the excitation energies  $E(k)$ s and excited eigenstates  $|\Phi_i(k)\rangle$ s at momentum  $k$ . In this work, we have employed an effective derivative trick and a regularization procedure, introduced in Ref. [63, 64], to determine the matrices that appear in Eq. (S-4).

As long as the wave functions of the excited states  $|\Phi_i(k)\rangle$ s are obtained, we can use them as a complete set to calculate the spin dynamical structure factor (DSF) ( $\alpha = x, y, z$ )

$$\begin{aligned} \mathcal{S}^{\alpha\alpha}(k, \omega) &= \int dt e^{-i\omega t} \langle \Psi_0 | S_{-k}^\alpha S_k^\alpha(t) | \Psi_0 \rangle \\ &= \sum_{mn} \int dt e^{-i(\omega + E_0)t} \langle \Psi_0 | S_{-k}^\alpha | \Phi_m(k) \rangle \langle \Phi_m(k) | e^{iHt} | \Phi_n(k) \rangle \langle \Phi_n(k) | S_k^\alpha | \Psi_0 \rangle \\ &= \sum_n \delta(E_n - E_0 - \omega) w_n^\alpha(k) \end{aligned} \quad (\text{S-5})$$

where  $w_n^\alpha(k) \equiv |\langle \Phi_n(k) | S_k^\alpha | \Psi_0 \rangle|^2$  is the spectral weight for each mode. If regarded as the overlap of two excited-state wave functions, the spectral weight can be tackled similarly by the derivative trick [64]. In practical calculations, a Lorentzian broadening is employed to deal with the delta function and mimic the finite temperature effect.

## LINEAR SPIN WAVE AND BOND-OPERATOR THEORIES FOR THE SS MODEL

To better understand the TN results in the antiferromagnetic (AFM) and the plaquette phases, we study the spin excitations in these two phases by using the linear spin wave (LSW) and bond-operator theories, respectively.

### Linear spin wave theory for spin excitations in the antiferromagnetic phase

Here we provide the LSW theory for spin excitations in the AFM phase of the SS model. We pick up a  $2 \times 2$  magnetic unit cell in the AFM state. Each spin on the SSL can be identified by the combination of a vector  $\mathbf{r}$  labeling the unit cell position and a sublattice index  $l$  ( $l = 1, 2, 3, 4$ ) within each unit cell. We introduce a unit vector  $\mathbf{n}_l$  to denote the orientation of the spin at sublattice  $l$ , and then define two additional unit vectors  $\mathbf{u}_l$  and  $\mathbf{v}_l$

according to  $\mathbf{u}_l \cdot \mathbf{n}_l = 0$  and  $\mathbf{v}_l = \mathbf{n}_l \times \mathbf{u}_l$ , namely,  $\mathbf{n}_l$ ,  $\mathbf{u}_l$  and  $\mathbf{v}_l$  are orthogonal to each other. Next we perform the Holstein-Primakoff transformation for the spin operator  $\mathbf{S}_{\mathbf{r}l}$ ,

$$\mathbf{n}_l \cdot \mathbf{S}_{\mathbf{r}l} = S - b_{\mathbf{r}l}^\dagger b_{\mathbf{r}l}, \quad (\text{S-6})$$

$$(\mathbf{u}_l + i\mathbf{v}_l) \cdot \mathbf{S}_{\mathbf{r}l} = (2S - b_{\mathbf{r}l}^\dagger b_{\mathbf{r}l})^{\frac{1}{2}} b_{\mathbf{r}l}, \quad (\text{S-7})$$

$$(\mathbf{u}_l - i\mathbf{v}_l) \cdot \mathbf{S}_{\mathbf{r}l} = b_{\mathbf{r}l}^\dagger (2S - b_{\mathbf{r}l}^\dagger b_{\mathbf{r}l})^{\frac{1}{2}}. \quad (\text{S-8})$$

Due to the bipartite lattice structure, we adopt two sets of Fourier transforms. On the sublattice  $l$  with an up spin:

$$b_{\mathbf{r}l} = \sqrt{\frac{2}{N}} \sum_{\mathbf{k} \in \text{MBZ}} b_{\mathbf{k}l} e^{i\mathbf{R}_{\mathbf{r}l} \cdot \mathbf{k}} \quad (\text{S-9})$$

and on the sublattice  $l'$  with a down spin:

$$b_{\mathbf{r}l'} = \sqrt{\frac{2}{N}} \sum_{\mathbf{k} \in \text{MBZ}} b_{\mathbf{k}l'} e^{-i\mathbf{R}_{\mathbf{r}l'} \cdot \mathbf{k}} \quad (\text{S-10})$$

where  $\mathbf{R}_{\mathbf{r}l}$  denotes the position of a spin on the SSL labeled by the magnetic unit cell position  $\mathbf{r}$  and sublattice index  $l$ . The spin Hamiltonian can be rewritten in terms of boson bilinears as

$$H_{\text{LSW}} = \sum_{\mathbf{k} \in \text{MBZ}} \Psi(\mathbf{k})^\dagger h(\mathbf{k}) \Psi(\mathbf{k}) + \text{const.}, \quad (\text{S-11})$$

where

$$\Psi(\mathbf{k}) = [b_{\mathbf{k}1}, b_{\mathbf{k}2}, b_{\mathbf{k}3}^\dagger, b_{\mathbf{k}4}^\dagger]^T, \quad (\text{S-12})$$

and

$$h(\mathbf{k}) = \begin{pmatrix} 2J - \frac{J'}{2} & \frac{J'}{2} e^{\frac{i(k_x - k_y)}{2}} & J \cos(\frac{k_x}{2}) & J \cos(\frac{k_y}{2}) \\ \frac{J'}{2} e^{-\frac{i(k_x - k_y)}{2}} & 2J - \frac{J'}{2} & J \cos(\frac{k_y}{2}) & J \cos(\frac{k_x}{2}) \\ J \cos(\frac{k_x}{2}) & J \cos(\frac{k_y}{2}) & 2J - \frac{J'}{2} & \frac{J'}{2} e^{-\frac{i(k_x + k_y)}{2}} \\ J \cos(\frac{k_y}{2}) & J \cos(\frac{k_x}{2}) & \frac{J'}{2} e^{\frac{i(k_x + k_y)}{2}} & 2J - \frac{J'}{2} \end{pmatrix}. \quad (\text{S-13})$$

Then we can diagonalize  $H_{\text{LSW}}$  via the Bogoliubov transformation with  $\Psi(\mathbf{k}) = T_{\mathbf{k}} \Phi(\mathbf{k})$ , where

$$\Phi(\mathbf{k}) = [\beta_{\mathbf{k}1}, \beta_{\mathbf{k}2}, \beta_{\mathbf{k}3}^\dagger, \beta_{\mathbf{k}4}^\dagger]^T, \quad (\text{S-14})$$

is the diagonalized basis and  $T_{\mathbf{k}}$  is the transformation matrix.

The general form of spin-wave dispersion is complex but can be easily computed numerically. Here we present the analytical form of the dispersions of the two Goldstone modes along the  $\Gamma$ -M direction near the  $\Gamma$  (and equivalently, M) point. Up to the second-order terms in the wave vector  $k_x = k_y$ , the dispersions for  $J \neq J'$  are

$$E_+ = \sqrt{\frac{2J^2(J-J')}{2J-J'}} k_x + \frac{J^2 J'}{2(2J-J')^2} k_x^2, \quad (\text{S-15})$$

$$E_- = \sqrt{\frac{2J^2(J-J')}{2J-J'}} k_x - \frac{J^2 J'}{2(2J-J')^2} k_x^2,$$

respectively. Note that the coefficients of the linear-in- $k_x$  terms are the same, while the splitting caused by the altermagnetism appears in the subleading  $k_x^2$  terms.

At  $J = J'$  where the AFM ground state becomes unstable in the LSW theory, these two magnon bands are softened with dispersion relations

$$E_+ = \frac{Jk_x^2}{2}, \quad (\text{S-16})$$

$$E_- = 0.$$

### Bond operator theory for the triplet excitations in the plaquette phase

In the plaquette phase, the spin rotational symmetry preserves and the LSW theory is not applicable. To derive the low-lying triplet excitations in this phase, we project the Hamiltonian onto the low-energy subspace composed of the singlet ground state and the lowest triplet excitations.

Define a vacuum  $|0\rangle$  state and four boson operators which yield the four physical states (one singlet and three triplets) by  $|s\rangle = s^\dagger|0\rangle$ ,  $|t_\alpha\rangle = t_\alpha^\dagger|0\rangle$ , respectively [77, 78]. The projection operators are expressed  $Z^{st_\alpha} = s^\dagger t_\alpha$ ,  $Z^{t_\alpha t_\beta} = t_\alpha^\dagger t_\beta$ . The spins represented via these boson operators are

$$S_l^\alpha = \frac{(-1)^l}{\sqrt{6}}(s^\dagger t_\alpha + t_\alpha^\dagger s) - \frac{i}{4} \sum_{\beta, \gamma} \epsilon_{\alpha\beta\gamma} t_\beta^\dagger t_\gamma \quad (\text{S-17})$$

where  $\alpha, \beta, \gamma = x, y, z$  denote the spin components and  $l$  is the sublattice index ( $l = 1, 2, 3, 4$ ). Note that the Hilbert space of the bosons is larger than the original plaquette Hilbert space and includes unphysical states. To restrict the boson Hilbert space to its physical sector, a hard-core constraint must be imposed:  $s^\dagger s + \sum_\alpha t_\alpha^\dagger t_\alpha = 1$ . By condensing the singlets  $s^\dagger = s \approx \langle s \rangle$ , we rewrite the Hamiltonian in terms of triplet operators

$$H = H_0 + \sum_{\mathbf{k} \in \text{MBZ}} \Psi(\mathbf{k})^\dagger h(\mathbf{k}) \Psi(\mathbf{k}) + \text{const.}, \quad (\text{S-18})$$

where  $H_0 = E_s s^\dagger s + \sum_\alpha E_\alpha t_\alpha^\dagger t_\alpha$  is the energy of a single plaquette and

$$\Psi(\mathbf{k}) = [t_{\mathbf{k}x}, t_{\mathbf{k}y}, t_{\mathbf{k}z}, t_{-\mathbf{k}x}^\dagger, t_{-\mathbf{k}y}^\dagger, t_{-\mathbf{k}z}^\dagger]^T \quad (\text{S-19})$$

Then following the standard Bogoliubov diagonalization we can derive the dispersion of the lowest triplet as

$$E = \sqrt{J^2 + \frac{2}{3}J(J' - 2J)(\cos(k_x) + \cos(k_y))}. \quad (\text{S-20})$$

We compare the triplet dispersion with that calculated by using the TN method in Fig. 3 of the main text, and they agree well. The small difference is likely caused by the finite bond dimension  $D$  in the TN calculation.

### NUMERICAL RESULTS ON THE SPIN EXCITATION SPECTRA

Here we show numerical results on the spin excitation spectra in addition to those in the main text. The spectra illustrate the spin DSF. In Fig. 2(b) we have shown the spectra in the AFM phase at  $J/J' = 1.1$  calculated in the TN approach with bond dimension  $D = 3$ . In Fig. S-2, we show calculated spectra for several other  $J/J'$  values and with different bond dimension  $D$ . One sees that the spectra show similar features with two split magnon bands, which are the Goldstone modes, at low energy and several longitudinal modes at high energy. Interestingly, the spin gap of the Higgs mode decreases with decreasing  $J/J'$  toward the plaquette-to-AFM transition, as discussed in the main text.

As an effect of finite  $D$ , the Goldstone modes exhibit a finite gap. We have calculated the spin gaps with other  $D$  values. As shown in Fig. S-3, the spin gap reduces with increasing  $D$  and eventually vanishes in the large  $D$  limit. This indicates that the gapless feature of Goldstone modes is captured by the tensor network calculation in this limit.

To show that the chiral magnon excitations in the AFM phase of the SS model, we calculate the difference of the transverse component of the DSF  $\Delta\mathcal{S} = \mathcal{S}^{+-}(\mathbf{q}, \omega) - \mathcal{S}^{-+}(\mathbf{q}, \omega)$ . Note that  $S_i^+ S_j^- - S_i^- S_j^+ \propto (\mathbf{S}_i \times \mathbf{S}_j)_z$ , so that the sign of  $\Delta\mathcal{S}$  is able to detect the chirality of the spin excitations. In Fig. S-4 we compare results of  $\Delta\mathcal{S}$  calculated by LSW theory and tensor network method. Both results show a finite splitting between the two Goldstone modes with opposite sign of  $\Delta\mathcal{S}$ . Also note that the magnon bands along  $\Gamma$ -M and  $\Gamma$ -M' also have opposite sign. Interestingly, we find that the optical magnon bands also exhibit opposite chirality. These results verify the existence of chiral magnons in the AFM state, which is caused by the symmetry of altermagnetism.

Besides the collective magnon excitations and the longitudinal modes, the tensor calculation also resolves continuum excitations. The spectral weights of these excitations are much smaller than the collective modes but as shown in Fig. S-5, they cause a broad peak in the density of states (DoS) at high energy. In the AFM phase, this broad peak appears in energies above the Higgs gap (above  $\sim 2J'$  at  $J/J' = 1.1$ ), and the peak energy decreases with varying  $J/J'$  toward the plaquette-to-AFM transition. This behavior is consistent with the emergence of deconfined excitations although it is hard to tell whether the continuum has a spinon or magnon origin. In the plaquette phase, we can

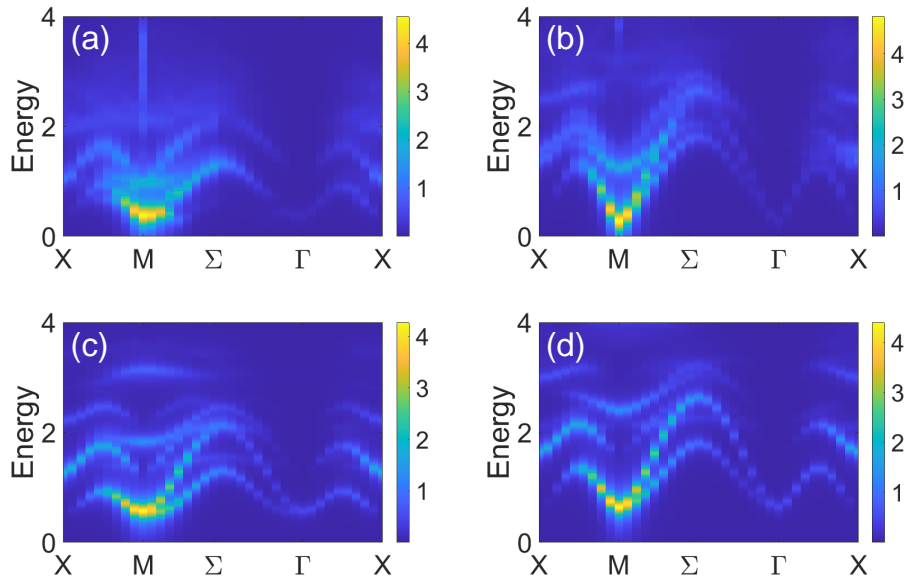


FIG. S-2. Total spin DSF ( $S^{xx+yy+zz}$ ) in the AFM phase of the SS model calculated by iPEPS method with  $D = 3$  (in (a) and (b)) and  $D = 2$  (in (c) and (d)), at  $J/J' = 0.9$  (in (a) and (c)) and  $J/J' = 1.1$  (in (b) and (d)).

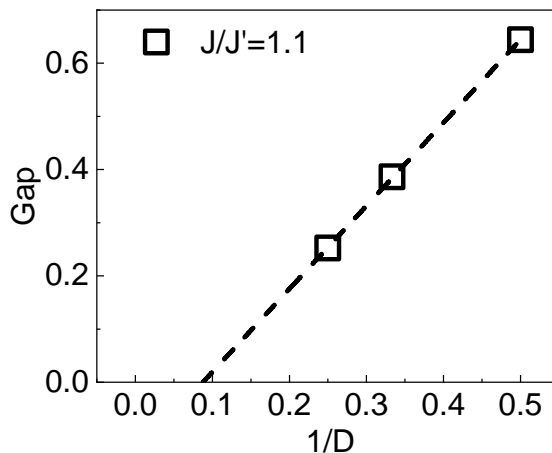


FIG. S-3. Finite  $D$  scaling of the spin gap of the Goldstone modes (at M point) in the AFM phase of the SS model at  $J/J' = 1.1$ . The dashed line shows a best fit to the gap, which vanishes in the large  $D$  limit.

also identify continuous excitations at energies above the triplet gap (above  $\sim J'$  at  $J/J' = 0.7$ ) in the DoS plots (Fig. S-5(b)). The behavior of energies of these excitations is similar to that in the AFM phase.

To understand the singlet and the 7-fold multiplet modes above the lowest triplet mode in the plaquette phase resolved by the tensor network calculation in the main text, we apply a small magnetic field to split the multiplets. We also compare our tensor network results with those from exact diagonalization on a four-spin plaquette with nearest neighbor Heisenberg interaction. As shown in Fig. S-6(a), the 7-fold quasi-degenerate excitations splits under a small field. The gaps of three modes are unchanged under the field, while the gaps of two modes increase with the field, gaps of another two modes decrease with the field. Note that the slopes of the gaps are the same for these modes, and they are also same to the slopes of the split lowest triplet excitations. These indicate that the 7-fold multiplet actually consists of one singlet and two degenerate triplets. This conclusion is further confirmed by our exact diagonalization calculation shown in Fig. S-6(b). At zero field, there are indeed 7-fold degenerate multiplet excitations above the triplet ones. With applying a small magnetic field, The 7-fold multiplet splits into a pair of

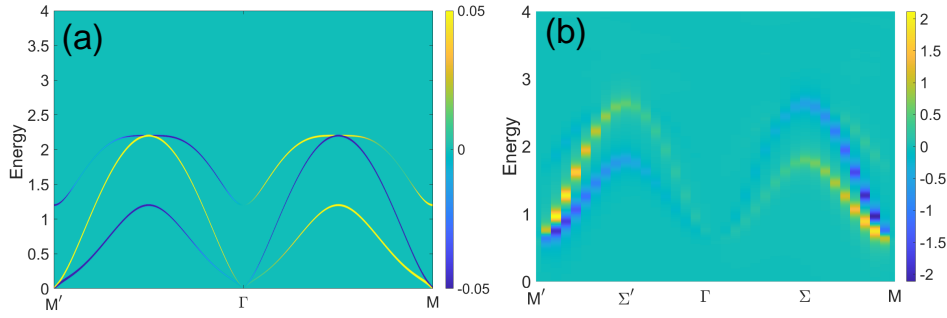


FIG. S-4. (a): Difference of the transverse DSF  $\Delta\mathcal{S} = \mathcal{S}^{+-}(\mathbf{q}, \omega) - \mathcal{S}^{-+}(\mathbf{q}, \omega)$  in the AFM phase of the SS model at  $J/J' = 1.1$  in the LSW theory. (b): Same as (a), but calculated by the tensor network method. In either case, the opposite sign of  $\Delta\mathcal{S}$  reflects the opposite chirality of the magnon modes.

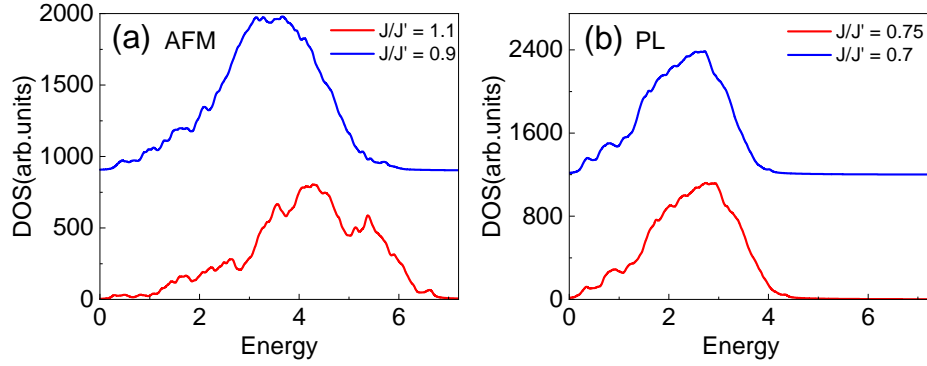


FIG. S-5. (a): Density of states (DoS) with excitation energy at several  $J/J'$  values in the AFM phase. (b): Same as (a) but in the plaquette phase.

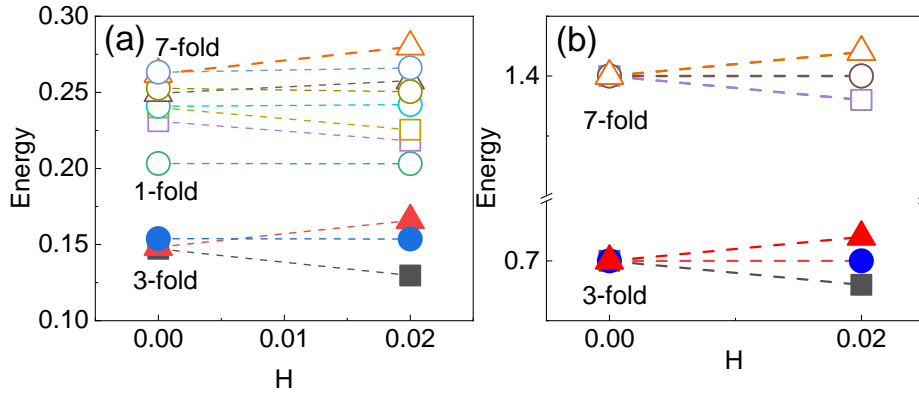


FIG. S-6. (a): Field dependence of gaps of several low-energy excitations in the plaquette phase of the SS model, calculated by the TN method. The multiplets split into  $S^z = +1, -1, 0$  states. (b): Field dependence of low-energy excitations of a 4-spin cluster with nearest neighbor AFM interactions, calculated by the ED. The splitting indicates that the 7-fold multiplet contains two degenerate triplets and one singlet.

triplets and one singlet. Note that the singlet excitation in between the lowest triplet and the 7-fold multiplet seen in the tensor network result in Fig. 3 of the main text does not show up in our 4-spin cluster exact diagonalization calculation. It is then interpreted as an inter-plaquette bound state.

In Fig. 4(a) of the main text we discuss the evolution of triplet mode, Higgs mode, and Goldstone modes with varying  $J/J'$ . It is found that the gaps of both triplet mode and Higgs mode drop rapidly to small values close to zero, and become quasi-degenerate with the Goldstone modes when approaching the plaquette-to-AFM transition. Here in Fig. S-7 we show results with several other bond dimension  $D$  values. We observe the same behavior that the



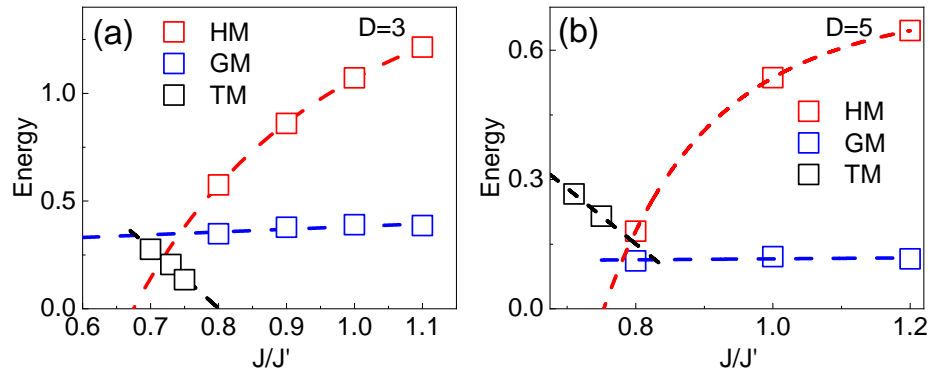


FIG. S-7. Evolution of gaps at the M point of the triplet mode (TM), Higgs mode (HM), and Goldstone modes (GM) with  $J/J'$  near the plaquette-to-AFM transition in the iPEPS calculation with  $D = 3$  (in (a)) and  $D = 5$  (in (b)). In either case we observe softening of gaps of both the triplet mode and Higgs mode when approaching the plaquette-to-AFM transition.

gaps of both triplet mode and Higgs mode are softened near the transition. This behavior strongly suggests emergence of nearly deconfined excitations at the plaquette-to-AFM transition.